Direct measurement of the density and energy level of compensating acceptors and their impact on the conductivity of n-type Ga_2O_3 films

Cite as: J. Appl. Phys. **127**, 145701 (2020); https://doi.org/10.1063/1.5143030 Submitted: 19 December 2019 . Accepted: 26 March 2020 . Published Online: 10 April 2020

Md Minhazul Islam 🗓, Naresh Adhikari, Armando Hernandez 🗓, Adam Janover 🗓, Steven Novak 🗓, Sahil Agarwal, Charles L. Codding, Michael Snure, Mengbing Huang 🗓, and Farida A. Selim 🗓











Direct measurement of the density and energy level of compensating acceptors and their impact on the conductivity of n-type Ga₂O₃ films

Cite as: J. Appl. Phys. **127**, 145701 (2020); doi: 10.1063/1.5143030 Submitted: 19 December 2019 · Accepted: 26 March 2020 · Published Online: 10 April 2020







Md Minhazul Islam, ^{1,2} Naresh Adhikari, Armando Hernandez, ^{1,2} Adam Janover, 0 Steven Novak, 0 Sahil Agarwal, 1,2 Charles L. Codding, 1 Michael Snure, 4 Mengbing Huang, 3 and Farida A. Selim 1,2,a) Sahil Agarwal, 1,2 Charles L. Codding, 1 Michael Snure, 4 Mengbing Huang, 3 and Farida A. Selim 1,2,a)

AFFILIATIONS

- ¹Center for Photochemical Sciences, Bowling Green State University, Bowling Green, Ohio 43403, USA
- ²Department of Physics and Astronomy, Bowling Green State University, Bowling Green, Ohio 43403, USA
- ³College of Nanoscale Science and Engineering, State University of New York Polytechnic Institute, Albany, New York 12203, USA
- ⁴Air Force Research Laboratory, Sensors Directorate, Wright Patterson AFB, Ohio 45433, USA

ABSTRACT

Intrinsic and extrinsic point defects often act as electron traps in oxide-based semiconductors and significantly impact their electrical and optical properties. Here, we show how to measure the density, energy level, and trapping cross section of the compensating acceptors that act as electron traps in Ga_2O_3 films, and we introduce the sheet trap number or the sheet compensating acceptor number as an essential parameter to fully describe the electrical transport properties of semiconductors. Si-doped β - Ga_2O_3 thin films were fabricated homoepitaxially by metalorganic chemical vapor deposition and studied by thermally stimulated luminescence spectroscopy, temperature dependent Hall-effect measurements, and secondary ion mass spectroscopy to investigate the compensating acceptor defects responsible for suppressing conductivity in the films. A deep level defect of energy in the range of 0.50–0.65 eV was identified as a compensating acceptor. The correlation between the electrical properties and its concentration and characteristics was established. This work shows how to quantify the density of compensating acceptors in semiconductors and directly relate it to the electrical transport properties, which should significantly advance the development of semiconductors and devices.

Published under license by AIP Publishing. https://doi.org/10.1063/1.5143030

I. INTRODUCTION

Ga₂O₃ is a transparent conducting oxide (TCO) with a wide energy bandgap (4.5–4.9). β -Ga₂O₃ is the most stable polymorph of Ga₂O₃ with a monoclinic crystal structure that belongs to the C2/m point group. ^{1,2} High breakdown voltage, high energy conversion efficiency together with high Baliga's Figure of Merit (BFOM) make it a powerful competitor for the next generation power electronics. ^{1–8} Besides, it has a potential use as a TCO due to having high transmittivity (in the range 300–1000 nm), low electron affinity, and a large energy bandgap. ⁹ Moreover, a low cost, low defect density β-Ga₂O₃ native substrate and the ability to grow large size substrates by a melt growth process (which is advantageous over the growth techniques of SiC and bulk GaN) make β-Ga₂O₃ a potential material for future low cost, high power

devices. ^{1,2} Several growth techniques of β -Ga₂O₃ including the Czochralski (CZ) method, ^{10,11} edge-defined film fed (EFG), ¹² and floating zone (FZ)^{13,14} have been reported for growing β -Ga₂O₃ substrates. EFG is the most suitable method for a growing β -Ga₂O₃ substrate where Si and Ir atoms from the β -Ga₂O₃ seed and crucible lead to the unintentionally doped (UID) n-type conductivity in the material. ¹² Deep acceptors such as Mg and Fe are commonly used to compensate those n-type dopants to achieve the semi-insulating property. ¹ Developing epitaxially grown β -Ga₂O₃ thin film is as important as the substrate to make this material suitable for device manufacturing. Some of the major challenges in the epitaxial growth of the thin film are control of dopants and minimization of defects and imperfections in a crystal lattice. The homoepitaxial growth of β -Ga₂O₃ is being carried out due to the availability of large size native substrates grown by different melt

^{a)}Author to whom correspondence should be addressed: faselim@bgsu.edu

growth methodology, and epitaxial films have been recently grown by Metalorganic Chemical Vapor Deposition (MOCVD), ¹⁵ molecular beam epitaxy (MBE), 16-18 halide vapor phase epitaxy (HVPE), 19-22 mist-CVD, and some other CVD techniques. 23,24 MOCVD and MBE are the most popular epitaxial growth methods that have been widely used for growing GaN and GaAs. One of the most important goals of current β-Ga₂O₃ studies is to attain good quality homoepitaxial films with controlled carrier concentration and high mobility. While β-Ga₂O₃ is insulating in its defect free form, several attempts have been made to dope it with different elements in order to increase carrier concentration. The carrier density of 10^{16} – 10^{19} cm³ has been reported for β -Ga₂O₃ doped with Sn and Ge grown by MBE, ^{25,26} Si and Sn by metalorganic vapor phase epitaxy (MOVPE), ^{27,28} and Sn by MOCVD. ²⁹ Gogova et al.³⁰ recently reported the growth of Si-doped β-Ga₂O₃ on a sapphire (0001) substrate by the MOVPE method, and the crystals were n-type with electron concentrations in the range from $10^{16} \, \text{cm}^{-3} \text{ to } 10^{18} \, \text{cm}^{-3}$.

Despite the fast advancement in Ga₂O₃ growth, intrinsic and extrinsic point defects remain a big challenge with a large impact on the optical and electrical properties of Ga₂O₃ as in other oxidebased semiconductors.^{31–35} These defects trap electrons and act as scattering centers as well. Due to the introduction of discontinuity into the crystal structure, they create localized energy states into the energy bandgap of the material, and as a result, the electrical conductivity can be significantly hindered due to the presence of these active carrier traps. There have been several reports of the trap study in bulk crystals using Deep Level Transient Spectroscopy (DLTS) and other optically and thermally stimulated defect $^{6-38}$ Trap levels in β-Ga $_2$ O $_3$ films grown by hydride vapor phase epitaxy (HVPE) and deep level defects in Ge-doped β-Ga₂O₃ layers grown by plasma assisted molecular beam epitaxy were also reported.^{39,40} Neal et al. have studied deep acceptors in Fe- and Mg-doped β-Ga₂O₃ using temperature dependent Hall-effect measurements and measured activation energies of 0.86 eV and 1.1 eV, respectively, which are responsible for the semiinsulating properties of the respective samples.⁴¹ Irmscher et al. have reported deep levels at 0.55 eV and 1.04 eV related to the Fe impurities and a more common deep acceptor level at 0.74 eV related to the gallium vacancy, V_{Ga} . We have recently reported deep levels in undoped, Fe-doped, and Mg-doped β-Ga₂O₃ bulk single crystals where a deep acceptor level at 0.62 eV has been shown to arise from Fe-doping in β-Ga₂O₃. Theoretical calculations including both standard density functional theory and hybrid functional calculations showed that group 1, group 2, and group 12 elements including Zn, Cu, Mg, Ca, and Be create deep acceptor levels in β-Ga₂O₃ and, therefore, are able to trap electrons acting as compensating acceptors in n-type β-Ga₂O₃. And N-doped β-Ga₂O₃ nanowires have been fabricated, and acceptor characteristics have been studied from a linear I-V plot using Pt electrodes. 45 Zhang et al. have studied N-doped β-Ga₂O₃ films deposited by an RF magnetron sputtering technique and reported the creation of acceptor levels due to the N-incorporation. En-doped β -Ga₂O₃ nanowires/an n-type β-Ga₂O₃ thin film p-n homojunction were made, and acceptor characteristics of Zn were confirmed from the rectified behavior of an I-V curve. 47 Wei et al. have also reported the deep acceptor characteristics of Zn in β-Ga₂O₃. ⁴⁸ Johnson et al.

have recently studied the compensating acceptor defect in Sn-doped $\beta\text{-}Ga_2O_3$ bulk crystals. 49 However, there has not been any report of the determination of the compensating defect concentration in Si-doped conductive $\beta\text{-}Ga_2O_3$ thin films and their direct correlation with the suppression of free carriers.

In this work, we studied MOCVD grown β-Ga₂O₃ thin films doped with Si atoms using a Thermally Stimulated Luminescence (TSL) technique and directly identified the compensating acceptor defect that reduces electrical conductivity by trapping electrons. The depth of traps, their capturing cross section, and their concentration were calculated from the TSL glow curve using two different mathematical modelings to confirm consistency. A strong correlation of the electrical conductivity and charge carrier concentration with TSL emission and trap concentration was established. This work shows how to quantify the density of compensating acceptors in semiconductors and directly relate it to the electrical transport properties. We thus introduce a new term, "the sheet trap number" (number of compensating acceptor/cm²) or "the sheet compensating acceptor," as a new parameter to the common electrical transport properties of semiconductors. We show that it is not possible to fully understand the transport phenomena in semiconductors without quantifying and characterizing this sheet trap number.

II. METHODS

A. Sample preparation

Homoepitaxial β-Ga₂O₃ thin films doped with Si were grown on CZ-grown semi-insulating Fe-doped β-Ga₂O₃ (010) substrates by a MOCVD thin film deposition system located at Bowling Green State University. The Fe-doped β-Ga₂O₃ substrates were diced to 5 × 5 mm pieces before film deposition. Trimethylgallium (TMG), pure oxygen, and silane (SiH₄) were used as the precursors for Ga, O, and Si, respectively. Argon gas is used to carry the TMG into the reaction chamber at a precise rate by digitally controlling the mass flow rate using Imperium software. The system uses a vertical showerhead reactor configuration together with a high rpm carrier rotation to achieve uniform deposition. The temperature inside the reactor was kept at 740 °C during the 3 h long growth process. CZ-grown β-Ga₂O₃ (010) substrates purchased from Kyma were cleaned, first, using a spin coater while spraying ethanol, isopropanol, and de-ionized water at different intervals and dried with N2. After that, the substrate was cleaned with acetone, ethanol, and de-ionized water in an ultrasonic bath and then dried with N2. Once the carrier is loaded with the substrate in place, the chamber was set to N₂ idle to seal the chamber in a vacuum before any recipes begin. Once the chamber is sealed completely, the recipe was run.

B. Hall measurements

Hall-effect measurements were performed using a MMR system. Four indium contacts were made in a square arrangement on the samples, and the contact area was kept as small as possible. The current–voltage linearity was checked every time before running Hall measurement, and the difference in current between contacts was below 10%. The measurements were performed at a constant magnetic field of 9300 G. A cryostat chamber, vacuum

pump, liquid helium, and Lake Shore 335 temperature controller were used in conjunction with the Hall system to control the sample temperature during the measurements. The samples were given sufficient time to be in thermal equilibrium with the cryostat chamber before running the measurements.

C. SIMS

Secondary Ion Mass Spectroscopy (SIMS) measurements were carried out using a PHI 6650 quadrupole-based SIMS instrument. Profiles were acquired using 5 keV Cs⁺ bombardment at an incidence angle of 60° from normal and detecting negative secondary ions. Conversion of ion counts to concentrations used a reference Ga₂O₃ sample with known Si contents. The depth scales were calibrated by measuring the analytical crater depths using a Dektak 150 stylus profilometer. The estimated error for the concentration and depth scales are 15% and 5%, respectively.

D. TSL spectroscopy

TSL spectroscopy was performed using a spectrometer that was built by one of the authors of this article and explained in detail elsewhere. 50-53 It should be mentioned that the TSL measurement does not require construction of any diode or contact unlike DLTS that requires forming a metal-semiconductor or a p-n junction where the transient capacitance is measured after carrier injection. In the case of TSL, the carrier is injected optically, and the electrons/holes get trapped in metastable traps, which require thermal energy to release the carrier. The sample was placed inside a chamber with a glass window that was cooled by liquid N₂ to 82 K. Next, the sample was irradiated with ionizing radiation using a Xenon lamp for 30 min. The spot diameter on the sample is 4 mm. After that, irradiation was stopped, and the sample was heated up linearly at a constant heating rate of 60 K/min. The emissions due to the release of carriers from the trap and recombination of charge carriers (electron and hole) were collected during the temperature sweep using a CCD detector. The mathematical model of TSL can be constructed from the Arrhenius equation, which states the probability of the release of an electron from a trap per unit time,

$$P = s \exp\left\{-\frac{E_{\rm D}}{kT}\right\},\tag{1}$$

where P is the probability of the electron release per unit time, s is the frequency factor (s⁻¹), T is the absolute temperature (K), k is the Boltzmann constant, and $E_{\rm D}$ is the thermal activation energy (eV) of the traps. This $E_{\rm D}$ is the energy difference between the trap energy level and conduction band minimum in the case of the electron trap. Assuming that every recombination will produce one photon of a specific wavelength depending on the nature of the recombination center, negligible re-trapping of electrons after the release and a linear heating rate, we applied the Randal and Williams formula⁵⁴ to describe the TSL emission intensity as

follows:

$$I(T) = n_0 \frac{s}{\beta} \exp\left\{-\frac{E_{\rm D}}{kT}\right\} \times \exp\left\{-\frac{s}{\beta}\right\}$$
$$\times \int_{T_0}^T \exp\left\{-\frac{E_{\rm D}}{kT'}\right\} dT'. \tag{2}$$

Here, I is the emission intensity, n_0 is the total number of trapped electrons at time t = 0, and β is the constant heating rate. This equation describes an asymmetric glow peak that is skewed in the low temperature side and more steeply falls in the high temperature side. However, if significant re-trapping occurs, the peak becomes more symmetric in shape. At the beginning of the TSL emission, the initial rise of the peak can be represented by the first exponential term in Eq. (2). Therefore, ln(I) vs 1/kT would form a straight line with the slope equal to E_D , the activation energy of the trap, for the initial 10%-20% of the data points. The intercept of the vertical axis would give the quantity $\ln\left(\frac{n_{0.5}}{\beta}\right)$ from which defect concentration, $\frac{n_0}{V}$ can be found (V is the volume of the sample illuminated) if the frequency factor s is known. We used a slightly different approach to calculate the frequency factor, s, independently, called the multiple heating rate method. The TSL intensity is maximum at T_m , where dI/dT becomes zero, and Eq. (2) can be written as follows:

$$\frac{\beta E_{\rm D}}{kT_m^2} = s \exp\left[-\frac{E_{\rm D}}{kT_m}\right]. \tag{3}$$

It is evident from the equation that the peak position is dependent on the heating rate if other parameters are kept constant. A linear fitting is possible between $\ln \frac{\beta}{T_m^2}$ and $\frac{1}{T_m}$ where the frequency factor s can be found from the intercept of the line with the vertical axis.

III. RESULTS AND DISCUSSIONS

Homoepitaxial $\beta\text{-}Ga_2O_3$ thin films doped with Si were investigated by the Hall measurement system to determine the electrical transport properties and SIMS to determine the dopant concentrations in the films. Table I presents the dopant concentration of Si measured by SIMS and the sheet resistance for four films. A large discrepancy between the Si concentration and sheet resistance is

TABLE I. Concentration of Si dopants in MOCVD grown thin films and their respective sheet resistance.

Sample	Ga/O ratio in the growth process	Si concentration (cm ⁻³)	Sheet resistance (ohm cm ⁻²⁾
Sample 1	6.36×10^{-4}	2.94×10^{21}	1.33×10^{3}
Sample 2	1.14×10^{-3}	1.37×10^{22}	1.19×10^4
Sample 3	1.14×10^{-3}	1.15×10^{22}	1.37×10^{9}
Sample 4	3.80×10^{-4}	1.44×10^{21}	3.22×10^{9}
Sample 5	6.36×10^{-4}	N/A	>10 ¹²

clear with six orders of magnitude difference in the sheet resistance between samples 1 and 4 and five orders of magnitude between samples 2 and 3 despite a similar Si concentration. Sample 1 is the highest conductive sample even though the dopant concentration of Si is lower than the other samples.

Temperature dependent Hall measurements were performed on sample 1 as it is the most conductive sample to investigate the dependence of the sheet resistance and sheet number (number of free electrons/cm²) on the temperature and identify the ionization region. The temperature of the sample was lowered to 20 K and then allowed to increase up to 430 K while measuring the electrical transport properties. There was an abrupt decrease in the sheet resistance and an increase in the sheet number observed at around 50 K, which is assumed to be related to the ionization of donor atoms (Fig. 1). Because of a large bandgap of around 4.9 eV, the conductivity does not change significantly at a higher temperature, and the carrier concentration remains almost constant up to 430 K. This behavior confirms Si as the sole source of conducting electrons.

In order to delve deeper to understand what causes the large carrier suppression in samples 3 and 4 despite a similar dopant concentration with other samples, we investigated the presence of defects. Various intrinsic and extrinsic point defects are known to affect the electrical properties of oxide-based semiconductors by forming compensating acceptors and trapping electrons. TSL is an excellent technique to investigate active electron traps in materials. Defects at different energy levels are first filled with electrons by the optical injection of the respective charge carrier at low temperatures. After the saturation of traps with electrons, the temperature is increased linearly, while optical emission is recorded as the trap release electrons. The traps start to release electrons at a specific temperature based on their energy levels. At first, the release

of carriers starts to increase gradually with the temperature, which soon starts to decrease as the number of trapped electrons decreases. Therefore, a peak shape appears for every trap level in the form of an emission intensity. This technique has been used to qualitatively characterize defects in several oxides, including $\beta\text{-}Ga_2O_3$ single crystals. $^{43,50-53,55-57}$ In this work, we used it to investigate active electronic defects in Si-doped $\beta\text{-}Ga_2O_3$ thin films. A deep electron trap was identified in Si-doped $\beta\text{-}Ga_2O_3$ thin films, which are responsible for suppressing electrical conductivity and, hence, acting as a compensating acceptor. The defect center was studied in detail, and its correlation with the electrical conductivity and carrier concentrations of the films was established.

We studied a number of undoped and Si-doped β-Ga₂O₃ thin films grown by MOCVD with a wide range of conductivity. The glow curves relating the temperature and intensity of the emission are plotted in Fig. 2. We used high quality CZ-grown Fe-doped β-Ga₂O₃ substrates (010) to grow a homoepitaxial thin film. Therefore, it is necessary to confirm that the glow peak is not coming from the substrate but from the film. Figure 2(a) includes a TSL emission of the substrate showing no glow peak. The absence of the glow peak in the substrates can be explained by the nonradiative recombination of electrons and holes for having a high concentration of Fe impurities added to achieve semi-insulating substrates. By raising the temperature linearly, at the rate of 60 K/ min from 78 K to 600 K, all samples, undoped and doped with Si, show a peak at around 300 K. The most conspicuous feature of the plots is the gradual increase of the emission intensity, which is the integral of the area under the glow peak, with the increase in the sheet resistance [Fig. 2(b)] as well as the rise of the peak height in Fig. 2(a) with increasing sheet resistance. The emission wavelength of the glow peak is shown in Fig. 2(c) for sample 4, which is at around 700 nm. All the samples have shown the same emission.

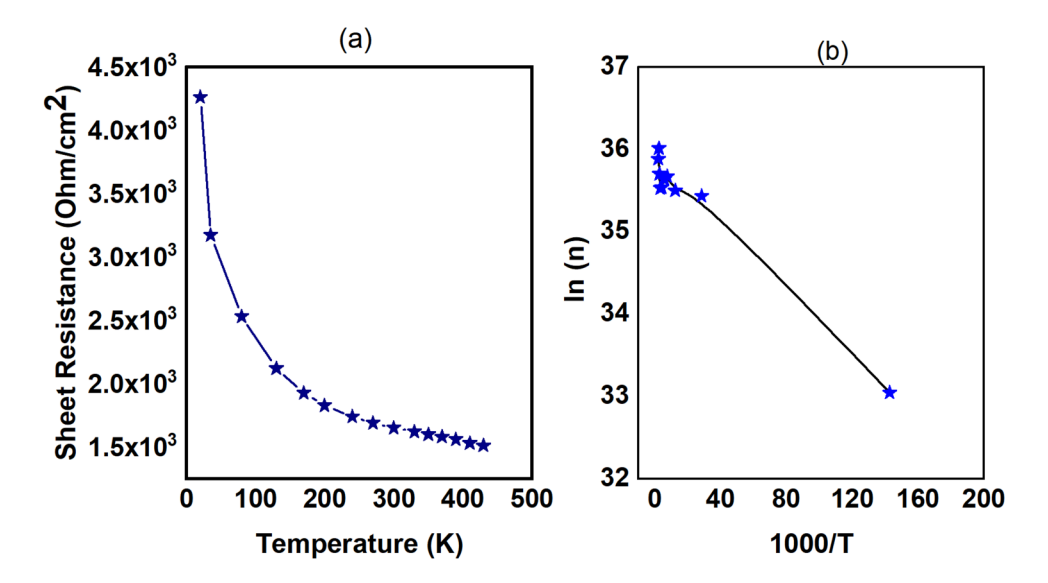


FIG. 1. Temperature dependent electrical transport properties of the most conductive sample. (a) Temperature dependence of the sheet resistance and (b) In of the sheet number (n) vs 1000/T.

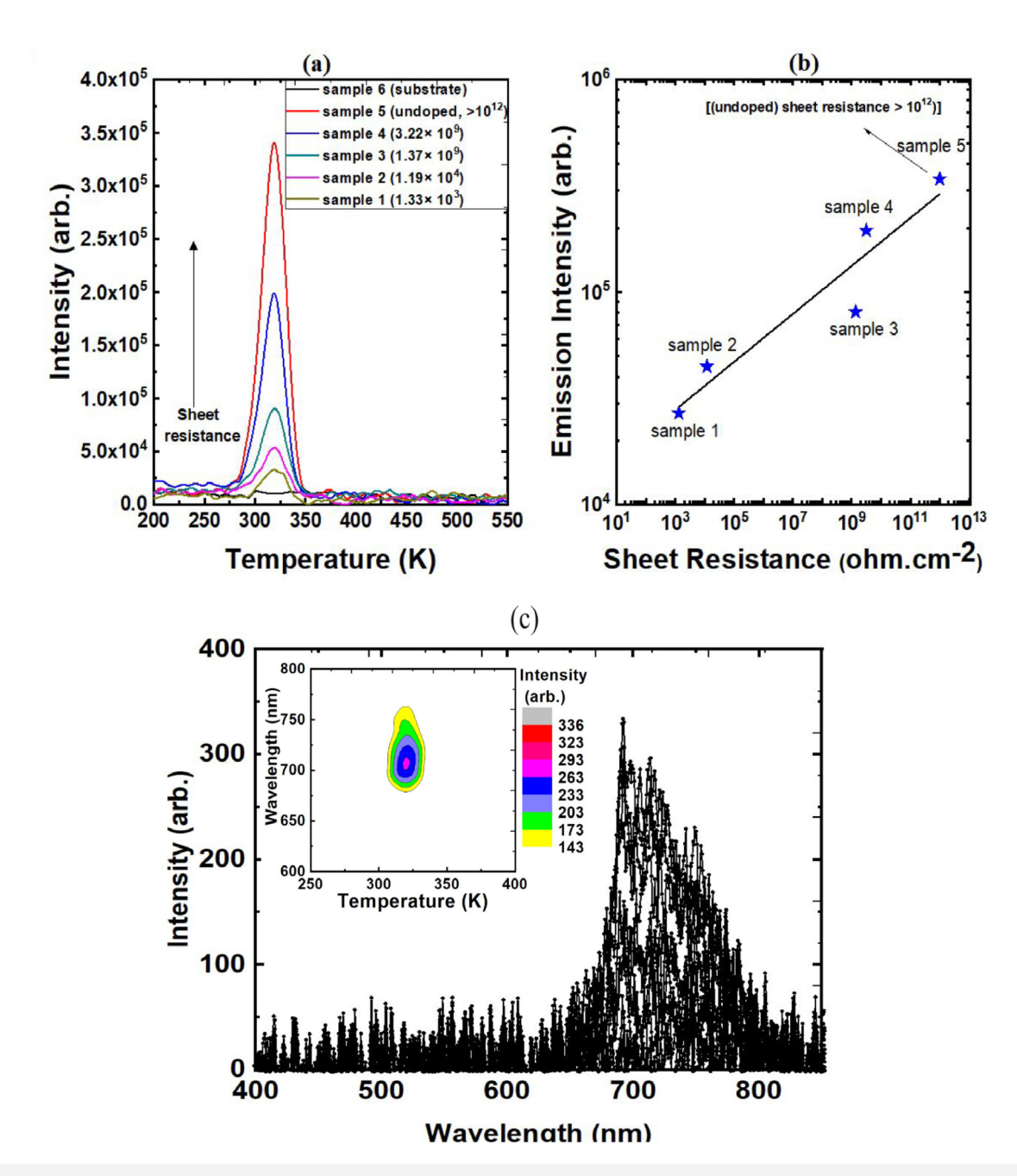


FIG. 2. TSL spectroscopy of β-Ga₂O₃. (a) Glow curve of different samples relating the temperature and emission intensity. (b) The change in the emission intensity with the sheet resistance of the samples. (c) Emission intensity as a function of the emission wavelength of the glow peak for sample 4.

This 700 nm emission has already been reported for β -Ga₂O₃. ⁴³ This red emission has been found to be due to the recombination of a localized electron and hole, which is deduced from the large stock shift of emission, hence strong electron–phonon coupling. ¹³ Nogales *et al.* have reported that the origin of red emission is the intrinsic defects of β -Ga₂O₃, not the impurities or extrinsic

dopants. 58 Therefore, the recombination center might be related to intrinsic defects in Ga_2O_3 .

Since the emission is due to the release of trapped carriers from the trap and every recombination gives one photon, the emission intensity is proportional to the trap concentration. Therefore, a clear dependence of the trap concentration and conductivity of

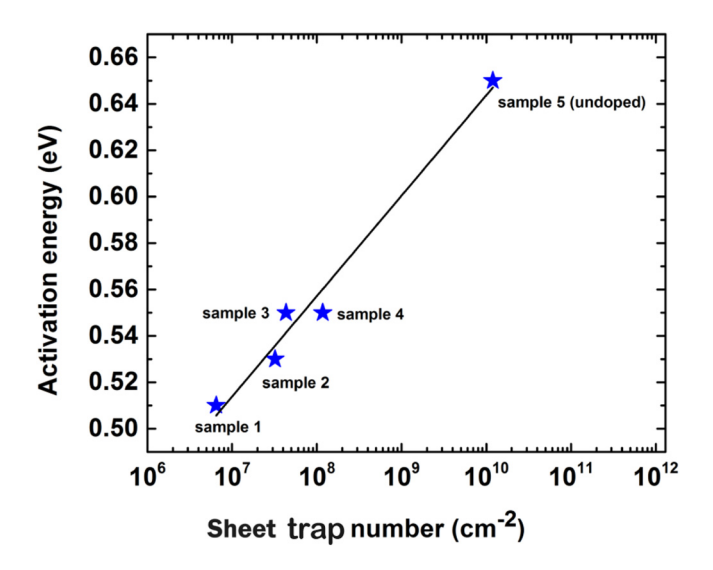


FIG. 3. Activation energy of the trap is plotted as a function of the sheet trap number.

the samples is evident. We investigated this donor compensating defect in detail to gain further information about its characteristics and energy level in the bandgap. By inspecting the glow curves (Fig. 2), we assumed first order kinetics because of the asymmetry of the curve, which indicates that no significant re-trapping occurred. We then used Eq. (2) to calculate the activation energy/ trap level of the traps and sheet trap number [Fig. 3, Table II]. The increase in activation energy can be explained by the increase in the defect concentration as reported for Fe-doped β -Ga₂O₃. ⁴¹

In order to find the frequency factor of the trap, which can be equated to capturing the cross section of the trap, we used Eq. (3) where four different heating rates, 30, 50, 90, and 120 K/min were used. The glow curves and linear fitting of $\ln \frac{\beta}{T_T}$ vs $\frac{1}{T_m}$ for sample 4 are shown in Fig. 4. The glow peak maximum moves to a higher temperature with the increase in heating rates but does not change the activation energy. The frequency factor and activation energy were found from the intercept of the vertical axis and the slope of the straight line, respectively.

We also calculated the activation energy by this method (multiple heating rates), which gives a very similar result (0.48 eV)

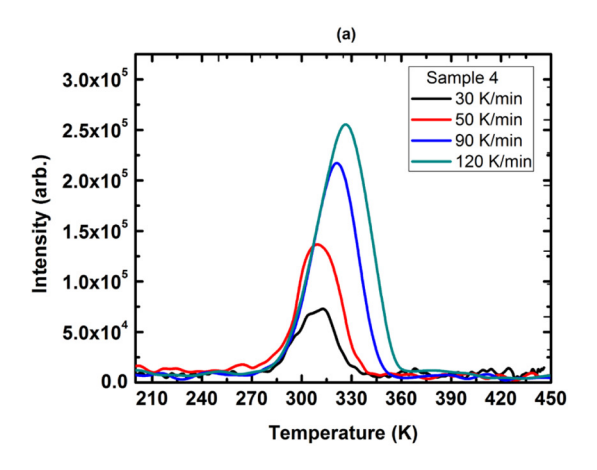
to the value calculated by Eq. (2). This gives confirmation that the assumption of first order kinetics was accurate as the "multiple heating rate" method is only applicable to first order kinetics. Equation (2) was then used in conjunction with Eq. (3) in Sec. II to calculate the sheet trap number. The results are shown in Table II. We introduce the term "Sheet trap number" to represent the number of compensating acceptors per cm² to compare with the sheet carrier number.

Figure 5 shows the relation of the sheet trap number, which represents the number of compensating acceptors per cm², with the sheet resistance (ohm cm²) and the sheet carrier number (cm²). The sheet trap number is maximum for the undoped film, which confirms that the origin of the trap is not related to Si doping. The conductivity decreases with the increase in the sheet trap number for Si-doped samples. It implies that Si increases the carrier concentration by acting as a shallow donor. However, the free carrier concentration also depends on the electron trap that suppresses conductivity by trapping them, exclusively acting as compensating acceptors.

The TSL technique, unlike DLTS, cannot directly tell if a trap is an electron or a hole trap. However, since Si acts as a shallow donor in β-Ga₂O₃³⁰ and this trap decreases the free carrier concentration by trapping electrons, it must act as a donor compensating acceptor. Deep trap levels of energy $\approx E_C$ of 0.50 to E_C of 0.65 eV have been identified in different melt grown β-Ga₂O₃ substrates. 40,43 Zhang et al. have reported an electron trap at E_c of 0.62 along with other common traps at E_c of 0.82 and E_c of 1.0 eV in EFG grown β-Ga₂O₃. However, the origin of the defects or the physical sources of these levels have not been discussed. Irmscher et al. have reported a compensating acceptor trap at 0.55 eV below the conduction band in a CZ-grown undoped β-Ga₂O₃ single crystal and assumed that the extrinsic impurities (Fe³⁺, Co³ might be responsible for the traps. 42 Therefore, the origin of this defect might be similar irrespective of the growth method. We have recently studied a β-Ga₂O₃ bulk single crystal where a trap level at 0.62 eV has been identified to be related to the Fe impurities.⁴³ Although we eliminate the possibility of Fe contamination from the MOCVD system that was used to grow the films, Fe impurities might diffuse from the substrate to the film during the high temperature growth process and act as an electron trap. Johnson et al. have recently studied the compensating acceptor defect in Sn-doped β-Ga₂O₃ bulk crystals with an energy level at 2.0 eV below the conduction band that involves a complex consisting of two V_{Ga} and an interstitial gallium. 49 Chikoidze et al. have reported

TABLE II. Defect parameters and electrical parameters of MOCVD grown β -Ga₂O₃ thin films.

Sample	Sheet resistance (ohm cm ⁻²)	Sheet carrier number (cm ⁻²)	Thermal activation energy, E_{D} (eV)	Frequency factor, S	Sheet trap number (cm ⁻²)
Sample 1	1.33×10^3 1.19×10^4	2.95×10^{15} 4.16×10^{14}	0.51 ± 0.10	3.42×10^6 3.42×10^6	6.48×10^6 3.21×10^7
Sample 2 Sample 3	1.37×10^{9}	8.05×10^{6}	$0.53 \pm 0.09 \\ 0.55 \pm 0.08$	3.42×10^{6} 3.42×10^{6}	4.33×10^{7}
Sample 4 Sample 5	3.22×10^9 >1.0 × 10 ¹²	2.90×10^6 < 1.0×10^3	0.55 ± 0.13 0.65 ± 0.12	3.42×10^6 3.42×10^6	1.17×10^8 1.19×10^{10}
(undoped)	>1.0 × 10	<1.0 × 10	0.03 ± 0.12	3.42 × 10	1.17 × 10



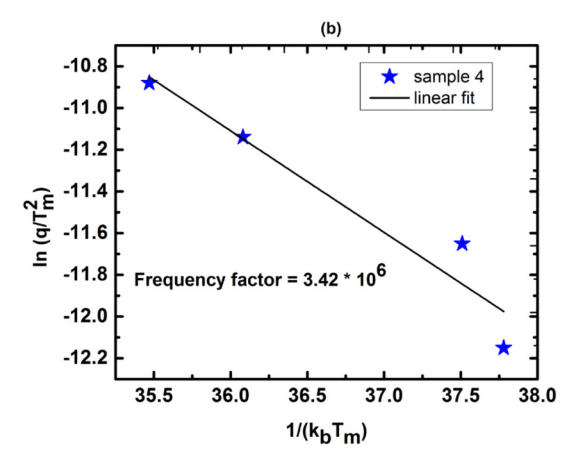


FIG. 4. Multiple heating rate method calculations of the activation energy and frequency factor of the traps. (a) Glow curve of sample 4 for four different heating rates. (b) Linear fitting of parameters used in the calculation of the frequency factor and activation energy.

that V_{Ga} is responsible for the p-type conductivity in uncompensated pulsed laser deposition grown β -Ga₂O₃/c-sapphire epi-wafers with an ionization energy at $1.12\,\text{eV}$. Moreover, V_{Ga} has a low formation energy under an oxygen rich condition with tetrahedral V_{Ga} formation energy slightly lower than the octahedral V_{Ga} .

Table I shows the Ga/O ratios that were used to grow the films. The V_{Ga} should increase with the decrease in the Ga/O ratio used for the growth because a decrease of the Ga/O ratio leads to O-rich and Ga-poor Ga_2O_3 films affecting the stoichiometry and leading to the formation of V_{Ga} . Si doping may also modify the formation energy of Ga vacancies and may induce complex defects.

From the aforementioned discussion, it is expected that the defect concentration and TSL emission should increase with the decrease in the Ga/O ratio. However, sample 2, which was grown with a higher Ga/O ratio than sample 1, exhibits a higher defect concentration. Moreover, samples 2 and 3 were grown with the same Ga/O ratio, though sample 3 exhibits a higher defect

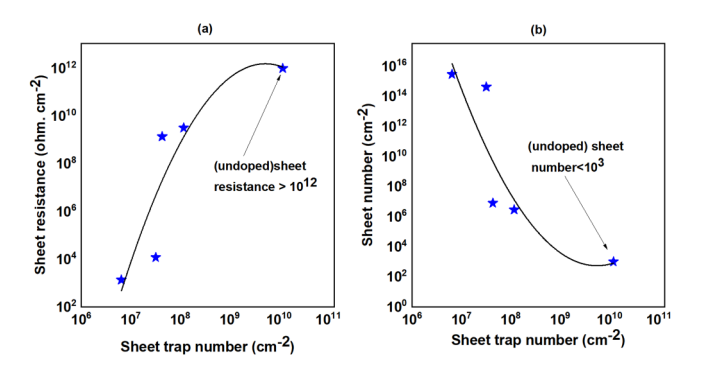


FIG. 5. The correlation between the sheet trap number (sheet compensating acceptors) and electrical transport properties: (a) sheet resistance and (b) sheet number (number of free electrons/cm²).

concentration than sample 2. The reason for that is both Fe and V_{Ga} act as compensating acceptors and are thus possible candidates for the defect center. While V_{Ga} may depend on the growth conditions and the Ga/O ratio, it is not possible to control Fe impurities. Although we expect that no contamination is present in the MOCVD reactor as discussed above, Ga₂O₃ substrates are often doped with different concentrations of Fe atoms. These Fe impurities may diffuse to the films during the high temperature growth and act as compensating acceptors. Several works reported that Fe impurities induce deep levels at approximately 0.60 eV, which indicates that the defect center here may be an Fe impurity as V_{Ga} may create deeper levels as mentioned above. 40,42,43,59 Therefore, Fe is probably responsible too for the compensating acceptor defect suppressing free electrons and, hence, increasing resistivity by trapping them. However, it is not possible to accurately determine the origin of compensating acceptors without further measurements. Positron annihilation spectroscopy, which is a powerful technique to investigate cation vacancy (e.g., V_{Ga}) type defects, can be used in future works to investigate the contribution of V_{Ga}. The focus of the current work is to only develop a method for measuring the sheet trap number and correlate it with the electrical transport properties, but it cannot provide direct information about the origins of the compensating acceptors.

IV. CONCLUSIONS

In summary, we have successfully characterized compensating acceptor defects in $\beta\text{-}Ga_2O_3$, which are primarily responsible for suppressing free carrier concentration and electrical conductivity in Si-doped Ga_2O_3 thin films. We introduced an important parameter, "the sheet trap number," to the common electrical transport properties to fully describe the electrical transport phenomena in semiconductors and show how to quantify it. This work reveals that the electrical conductivity and charge carrier concentration are strongly dependent on this number.

ACKNOWLEDGMENTS

The authors would like to thank Colin Wadsworth at the SUNY Polytechnic Institute for helping with SIMS measurements. This work was supported by a Building Strength grant from Bowling Green State University.

REFERENCES

- ¹H. Zhou, J. Zhang, C. Zhang, Q. Feng, S. Zhao, P. Ma, and Y. Hao, J. Semicond. **40**, 011803 (2019).
- ²S. I. Stepanov, V. I. Nikolaev, V. E. Bougrov, and A. E. Romanov, Rev. Adv. Mater. Sci. 44, 63-86 (2016).
- ³K. D. Chabak, N. Moser, A. J. Green, D. E. Walker, S. E. Tetlak, E. Heller, A. Crespo, R. Fitch, J. P. McCandless, K. Leedy, M. Baldini, G. Wagner, Z. Galazka, X. Li, and G. Jessen, Appl. Phys. Lett. 109, 213501 (2016).
- ⁴Y. Zhang, C. Joishi, Z. Xia, M. Brenner, S. Lodha, and S. Rajan, Appl. Phys. Lett. 112, 233503 (2018).
- ⁵M. J. Tadjer, N. A. Mahadik, V. D. Wheeler, E. R. Glaser, L. Ruppalt, A. D. Koehler, K. D. Hobart, C. R. Eddy, and F. J. Kub, ECS J. Solid State Sci. Technol. 5, P468 (2016).
- ⁶A. J. Green, K. D. Chabak, E. R. Heller, R. C. Fitch, M. Baldini, A. Fiedler, K. Irmscher, G. Wagner, Z. Galazka, S. E. Tetlak, A. Crespo, K. Leedy, and G. H. Jessen, IEEE Electron Device Lett. 37, 902 (2016).
- ⁷K. Zeng, J. S. Wallace, C. Heimburger, K. Sasaki, A. Kuramata, T. Masui, J. A. Gardella, and U. Singisetti, IEEE Electron Device Lett. 38, 513 (2017).
- ⁸B. J. Baliga, IEEE Electron Device Lett. 10, 455 (1989).
- ⁹S. C. Siah, R. E. Brandt, K. Lim, L. T. Schelhas, R. Jaramillo, M. D. Heinemann, D. Chua, J. Wright, J. D. Perkins, C. U. Segre, R. G. Gordon, M. F. Toney, and T. Buonassisi, Appl. Phys. Lett. 107, 252103 (2015).
- 10Z. Galazka, K. Irmscher, R. Uecker, R. Bertram, M. Pietsch, A. Kwasniewski, M. Naumann, T. Schulz, R. Schewski, D. Klimm, and M. Bickermann, J. Cryst. Growth 404, 184 (2014).
- 11 Z. Galazka, R. Uecker, K. Irmscher, M. Albrecht, D. Klimm, M. Pietsch, M. Brützam, R. Bertram, S. Ganschow, and R. Fornari, Cryst. Res. Technol. 45, 1229 (2010).
- 12A. Kuramata, K. Koshi, S. Watanabe, Y. Yamaoka, T. Masui, and S. Yamakoshi, Jpn. J. Appl. Phys. 55, 1202A2 (2016).
- 13 J. Zhang, B. Li, C. Xia, G. Pei, Q. Deng, Z. Yang, W. Xu, H. Shi, F. Wu, Y. Wu, and J. Xu, J. Phys. Chem. Solids 67, 2448 (2006).
- ¹⁴N. Suzuki, S. Ohira, M. Tanaka, T. Sugawara, K. Nakajima, and T. Shishido, Phys. Status Solidi C 4, 2310 (2007).
- 15 F. Alema, B. Hertog, A. Osinsky, P. Mukhopadhyay, M. Toporkov, and W. V. Schoenfeld, J. Cryst. Growth 475, 77 (2017).
- 16H. Okumura, M. Kita, K. Sasaki, A. Kuramata, M. Higashiwaki, and J. S. Speck, Appl. Phys. Express 7, 095501 (2014).
- ¹⁷T. Oshima, N. Arai, N. Suzuki, S. Ohira, and S. Fujita, Thin Solid Films 516, 5768 (2008).
- ¹⁸T. Oshima, T. Okuno, and S. Fujita, Jpn. J. Appl. Phys. **46**, 7217 (2007).
- ¹⁹K. Nomura, K. Goto, R. Togashi, H. Murakami, Y. Kumagai, A. Kuramata, S. Yamakoshi, and A. Koukitu, J. Cryst. Growth 405, 19 (2014).
- 20 T. Watahiki, Y. Yuda, A. Furukawa, M. Yamamuka, Y. Takiguchi, and S. Miyajima, Appl. Phys. Lett. 111, 222104 (2017).

 ²¹Y. Oshima, E. G. Villora, and K. Shimamura, Appl. Phys. Express 8, 055501
- ²²H. Murakami, K. Nomura, K. Goto, K. Sasaki, K. Kawara, Q. T. Thieu, R. Togashi, Y. Kumagai, M. Higashiwaki, A. Kuramata, S. Yamakoshi, B. Monemar, and A. Koukitu, Appl. Phys. Express 8, 015503 (2014).
- ²³K. Akaiwa and S. Fujita, Jpn. J. Appl. Phys. **51**, 070203 (2012).
- ²⁴G. T. Dang, T. Kawaharamura, M. Furuta, and M. W. Allen, IEEE Electron Device Lett. 36, 463 (2015).
- ²⁵K. Sasaki, A. Kuramata, T. Masui, E. G. Víllora, K. Shimamura, and S. Yamakoshi, Appl. Phys. Express 5, 035502 (2012).

- 26 E. Ahmadi, O. S. Koksaldi, S. W. Kaun, Y. Oshima, D. B. Short, U. K. Mishra, and J. S. Speck, Appl. Phys. Express 10, 041102 (2017).

 27 M. Baldini, M. Albrecht, A. Fiedler, K. Irmscher, D. Klimm, R. Schewski, and
- G. Wagner, J. Mater. Sci. 51, 3650 (2016).
- 28 M. Baldini, M. Albrecht, A. Fiedler, K. Irmscher, R. Schewski, and G. Wagner, ECS J. Solid State Sci. Technol. 6, Q3040 (2017).
- 29 X. Du, Z. Li, C. Luan, W. Wang, M. Wang, X. Feng, H. Xiao, and J. Ma, . Mater. Sci. **50**, 3252 (2015).
- 30D. Gogova, G. Wagner, M. Baldini, M. Schmidbauer, K. Irmscher, R. Schewski, Z. Galazka, M. Albrecht, and R. Fornari, J. Cryst. Growth 401, 665
- 31 M. Yamaga, E. G. Villora, K. Shimamura, N. Ichinose, and M. Honda, Phys. Rev. B 68, 155207 (2003).
- 32 S. I. Maximenko, L. Mazeina, Y. N. Picard, J. A. Freitas, V. M. Bermudez, and S. M. Prokes, Nano Lett. 9, 3245 (2009).
- 33 E. Korhonen, F. Tuomisto, D. Gogova, G. Wagner, M. Baldini, Z. Galazka, R. Schewski, and M. Albrecht, Appl. Phys. Lett. 106, 242103 (2015).
- 34 J. B. Varley, J. R. Weber, A. Janotti, and C. G. Van de Walle, Appl. Phys. Lett. 97, 142106 (2010).
- 35 J. B. Varley, H. Peelaers, A. Janotti, and C. G. V. de Walle, J. Phys. Condens. Matter 23, 334212 (2011).
- ³⁶Z. Zhang, E. Farzana, A. R. Arehart, and S. A. Ringel, Appl. Phys. Lett. 108, 052105 (2016).
- 37_{M. E. Ingebrigtsen, L. Vines, G. Alfieri, A. Mihaila, U. Badstübner,} B. G. Svensson, and A. Kuznetsov, MSF 897, 755 (2017).
- 38Y. Nakano, ECS J. Solid State Sci. Technol. 6, P615 (2017).
- ³⁹A. Y. Polyakov, N. B. Smirnov, I. V. Shchemerov, E. B. Yakimov, S. J. Pearton, C. Fares, J. Yang, F. Ren, J. Kim, P. B. Lagov, V. S. Stolbunov, and A. Kochkova, Appl. Phys. Lett. 113, 092102 (2018).
- ⁴⁰E. Farzana, E. Ahmadi, J. S. Speck, A. R. Arehart, and S. A. Ringel, J. Appl. Phys. 123, 161410 (2018).
- 41 A. T. Neal, S. Mou, S. Rafique, H. Zhao, E. Ahmadi, J. S. Speck, K. T. Stevens, J. D. Blevins, D. B. Thomson, N. Moser, K. D. Chabak, and G. H. Jessen, Appl. Phys. Lett. 113, 062101 (2018).
- ⁴²K. Irmscher, Z. Galazka, M. Pietsch, R. Uecker, and R. Fornari, J. Appl. Phys. 110, 063720 (2011).
- 43M. M. Islam, D. Rana, A. Hernandez, M. Haseman, and F. A. Selim, J. Appl. Phys. 125, 055701 (2019).
- ⁴⁴A. Kyrtsos, M. Matsubara, and E. Bellotti, Appl. Phys. Lett. 112, 032108 (2018).
- 45L. L. Liu, M. K. Li, D. Q. Yu, J. Zhang, H. Zhang, C. Qian, and Z. Yang, Appl. Phys. A 98, 831 (2010).
- 46 Y. Zhang, J. Yan, Q. Li, C. Qu, L. Zhang, and T. Li, Phys. B 406, 3079
- ⁴⁷Q. Feng, J. Liu, Y. Yang, D. Pan, Y. Xing, X. Shi, X. Xia, and H. Liang, . Alloys Compd. 687, 964 (2016).
- ⁴⁸Y. Wei, Y. Jinliang, W. Jiangyan, and Z. Liying, J. Semicond. 33, 073003 (2012).
- ⁴⁹J. M. Johnson, Z. Chen, J. B. Varley, C. M. Jackson, E. Farzana, Z. Zhang, A. R. Arehart, H.-L. Huang, A. Genc, S. A. Ringel, C. G. Van de Walle, D. A. Muller, and J. Hwang, Phys. Rev. X 9, 041027 (2019).
- 50D. T. Mackay, C. R. Varney, J. Buscher, and F. A. Selim, J. Appl. Phys. 112, 023522 (2012).
- ⁵¹S. M. Reda, C. R. Varney, and F. A. Selim, Results Phys. 2, 123 (2012).
- 52 F. A. Selim, A. Khamehchi, D. Winarski, and S. Agarwal, Opt. Mater. Express 6, 3704 (2016).
- 53 F. Selim, inventor, "Methods and systems for testing luminescent semiconductors," U.S. patent application 15/141,808 (June 25, 2019).
- 54K. Mahesh, Thermoluminescence in Solids and Its Applications (Nuclear Technology Publishing, Ashford, UK, 1989).
- 55P. Saadatkia, C. Varney, and F. Selim, in Luminescence—An Outlook on the Phenomena and Their Applications, edited by J. Thirumalai (IntechOpen,

⁵⁶V. Pagonis, G. Kitis, and C. Furetta, Numerical and Practical Exercises in Thermoluminescence (Springer-Verlag, New York, 2006). 57. J. Ji, L. A. Boatner, and F. A. Selim, Appl. Phys. Lett. 105, 041102 (2014).

⁵⁸E. Nogales, B. Méndez, and J. Piqueras, Appl. Phys. Lett. 86, 113112

⁵⁹ E. Chikoidze, A. Fellous, A. Perez-Tomas, G. Sauthier, T. Tchelidze, C. Ton-That, T. T. Huynh, M. Phillips, S. Russell, M. Jennings, B. Berini,

F. Jomard, and Y. Dumont, Mater. Today Phys. 3, 118 (2017). ⁶⁰M. E. Ingebrigtsen, A. Y. Kuznetsov, B. G. Svensson, G. Alfieri, A. Mihaila, U. Badstübner, A. Perron, L. Vines, and J. B. Varley, APL Mater. 7, 022510 (2018).